A laser probe measurement of cavitation bubble dynamics improved by shock wave detection and compared to shadow photography

Rok Petkovšek[a] and Peter Gregorčič
Faculty of Mechanical Engineering, University of Ljubljana, Aškerčeva 6, 1000 Ljubljana, Slovenia

(Received 6 June 2007; accepted 11 July 2007; published online 31 August 2007)

High-intensity light from a laser pulse can produce optical breakdown in a liquid, followed by a shock wave and the growth of a cavitation bubble. When the bubble reaches its maximum radius the liquid pressure causes it to collapse, which in turn initiates the growth of another bubble. The oscillations can repeat themselves several times, and a shock wave is emitted after every collapse. In our study the breakdown was induced in distilled water by a Nd:YAG pulsed laser, which was designed for ocular photodisruption. The main focus of our experiments was measurement of the cavitation bubble and the shock waves using an optical probe based on deflections of a laser beam. The applied experimental setup made it possible to carry out one- or two-dimensional scanning of the cavitation bubble based on automatic control of the experiment. Since the beam-deflection probe (BDP) allowed simultaneous measurements of the cavitation bubble and the shock waves, we developed a method for reducing the measurement noise of the BDP scanning. This improvement includes an analysis of the secondary shock waves and leads to a significant reduction in the noise of the measurement. Simultaneous measurements based on shadow photography were used as a comparative method during the experiment. © *2007 American Institute of Physics*.
[DOI: 10.1063/1.2774000]

I. INTRODUCTION

The interest in studying cavitation-bubble oscillations comes from many fields. These oscillations are interesting because of their mostly unwanted, destructive effect on solid surfaces (erosion);[1–3] however, this effect can also be put to use in the interesting application of laser cleaning.[4] Study of cavitation-bubble oscillations is also potentially interesting for laser-based noncontact underwater communications[5] as well as for underwater explosions.[6] Many studies are dedicated to medical applications, especially in ophthalmology[3,7–12] and biomedicine, where cavitation of the microbubbles can be used to enhance membrane permeabilization and molecular uptake (sonoporation).[13,14] Because of this interest in cavitation bubbles—especially the dynamics and the associated mechanisms—different authors have developed a variety of experimental techniques. These techniques are focused on measuring the spreading and the oscillations of the bubbles. However, it is also important that the conditions for the bubble generation are well controlled, since the appearance of a cavitation bubble is statistical in nature, both in terms of location and time.[1]

Cavitation bubbles can be induced in different ways; however, laser-induced cavitation[1–5,7–12,15–23] is probably the most frequently employed method for the generation of bubbles due to its ability to accurately position the origin of the cavitation bubbles in space, as well as in time. However, other commonly used methods include acoustic generation[13,24,25] and spark-generated cavitation.[6,26]

There are several optical methods for measuring cavitation bubbles and the accompanying shock waves, such as a shadow photography,[8,11,16,18] high-speed photography,[1–3,9,12,15,17,20,21,26] streak photography,[18,19,27] schlieren photography,[17,27,28] holography-based photography,[24,29] measurements based on a laser-beam deflection probe (BDP),[10,17,22,30] and combinations of these methods. Methods based on electromechanical detectors (such as a hydrophone) have also been used;[3,7,12,16–18,21,25] however, electromechanical sensors are appropriate for far-field measurements and, as a result, they are not interesting for measurements of bubble dynamics, since the very high pressures of the shock waves in the vicinity of the breakdown region limit the application of such sensors because of their relatively low damage threshold. For this reason they have been used in combination with some of the optical methods as a reference[3,12,16–18] or as an independent measuring method in applications such as an investigation of the stochastic nature of cavitation[25] and measurements of the cavitation bubble's collapse time,[7,21] i.e., the time between the two pressure fronts accompanying the breakdown and the collapse of the cavitation bubble. Since the time between a bubble's appearance and its collapse is related by the Rayleigh formula,[31] it is possible to indirectly measure the radius of a bubble.

The main goal of our study was to develop simultaneous measurements of laser-induced cavitation bubbles by analyzing the deflections of a laser probe and by using shadow photography as a comparison. The accompanying shock waves were also detected and included in the signal processing and analysis.

To measure the time dependence of the cavitation bubble's radius we used a purpose-built positioning system, which allowed us to carry out one- or two-dimensional scanning based on probe-beam shifting in two dimensions. Spe-

[a]Electronic mail: rok.petkovsek@fs.uni-lj.si

cially developed software made it possible to control the experiment automatically as well as to acquire and process the data.

Since we used a scanning procedure, the bubble dynamics' measurements required us to repeat the process. Therefore, bubble scanning with the BDP as well as shadow photography involved successive laser-induced bubbles. In the case of BDP scanning, the measurements were made at different positions relative to the breakdown region, representing the origin of the cavitation bubble. On the other hand, the shadow photography was done at different times relative to the occurrence of breakdown. Although laser-induced breakdown ensures good repeatability, the variation in the breakdown laser energy as well as the statistical nature of cavitation increase the noise of the measurements. It is important to note that the technique based on the BDP allowed simultaneous measurements of the cavitation bubble and the shock waves—from one BDP signal all the bubble expansions, collapses, and shock waves can be obtained. Using this unique property of the BDP, we developed a method of data processing based on detecting the secondary shock waves. This method led to reductions in the measurement noise and, therefore, contributed to a significant improvement in the accuracy of the measurements of the bubble's dynamics for the first three bubble oscillations.

II. THEORY

The method, presented in Sec. IV, is based on the Rayleigh-Plesset theory.[31,32] Although this is a relatively simple model for cavitation-bubble dynamics, it does give important results, such as the bubble's oscillation time is proportional to the maximum radius, and that the general equation of motion for spherical bubbles in a liquid can be written in dimensionless form. This model agreed with experimental results and we used it in our method to reduce the measurement noise resulting from the BDP's scanning procedure.

A. Bubble's collapse and energy

A bubble's collapse in an infinitely large and incompressible liquid is roughly described by the Rayleigh model,[31] which considers that the liquid's pressure as well as the pressure inside the bubble is constant during its collapse. With this assumption Rayleigh deduced the variation of the bubble's radius with time from the kinetic energy of the motion and the work done by the pressure,

$$U^2 = \frac{2p_0}{3\rho}\left(\frac{R_{\max}^3}{R^3} - 1\right), \tag{1}$$

where $U = \mathrm{d}R/\mathrm{d}t$ is the velocity of the bubble's boundary, $R_{\max}$ is the maximum radius, p_0 is the liquid's pressure, and ρ is the liquid's density.

The bubble's collapse time can be obtained by integrating Eq. (1), and is expressed as

$$T_C = \sqrt{\frac{3\rho}{2p_0}}\int_0^{R_{\max}} \frac{(R/R_{\max})^{3/2}}{(1 - R^3/R_{\max}^3)^{1/2}}\mathrm{d}R$$

$$= 0.915\, R_{\max}\sqrt{\frac{\rho}{p_0}}. \tag{2}$$

From this we can see that the collapse time of a spherical cavitation bubble in an infinite liquid is proportional to its maximum radius. Even though the Rayleigh model is a relatively simple model for cavitation-bubble oscillations, Eq. (2), which describes the relationship between the collapse time and the maximum radius, it is still used by many authors.[2,3,6,7,9,12,17,26] Assuming that the expansion and collapse of the bubble are symmetrical processes, the oscillation time T_o, i.e., the time between the bubble's appearance and its collapse, can be expressed as $T_o = 2T_C$. This assumption is valid when the duration of the laser pulse is much shorter than the bubble's oscillation and the viscosity of the liquid is negligible.[8] In our experiments, both conditions were satisfied.

A cavitation bubble's energy, E_B, is proportional to the cube of its maximum radius,[5,33]

$$E_B = \frac{4\pi p_0}{3}R_{\max}^3. \tag{3}$$

A bubble's energy is also approximately proportional to the energy of the breakdown pulse, E_l,[7,12,33,34] so

$$E_B = \eta E_l. \tag{4}$$

Here, η is the share of the pulse's energy converted into the bubble's energy.

B. Rayleigh-Plesset equation

In 1949 Plesset[32] completed Rayleigh's model. His theory still assumed an incompressible and nonviscous liquid, but he started with the equation of continuity and the Navier-Stokes equation. If the radius of the bubble at any time t is R, and r is the radius at any point of the liquid, the velocity potential for motion of the liquid with spherical symmetry is

$$\phi = \frac{R^2\dot{R}}{r}. \tag{5}$$

It is well known that the Navier-Stokes equation for an incompressible liquid ($\nabla \cdot \mathbf{v} = 0$) can be written as

$$\rho\left(\frac{\partial \mathbf{v}}{\partial t} + (\mathbf{v}\cdot\nabla)\mathbf{v}\right) = \mathbf{f} - \nabla p + \mu\nabla^2\mathbf{v}. \tag{6}$$

Since the buoyancy force and gravity are negligible, the term $\mathbf{f}$, denoting the density of the external forces, should be zero, as should the last term in Eq. (6), denoting the viscosity. Considering an irrotational flow ($\nabla \times \mathbf{v} = 0$) and the relationship between the velocity and its potential ($\mathbf{v} = -\nabla\phi$), Eq. (6) gives

$$\nabla\left(-\frac{\partial\phi}{\partial t}+\frac{1}{2}(\nabla\phi)^2\right)=-\frac{\nabla p}{\rho}. \tag{7}$$

For a constant density, the integration of Eq. (7) gives

$$-\frac{\partial\phi}{\partial t}+\frac{1}{2}(\nabla\phi)^2=-\frac{p(r,t)}{\rho}+C(t), \tag{8}$$

where $C(t)$ represents the integration constant, which can be obtained from the boundary condition: if $r=\infty$ then $p=p_0$. This gives the Bernoulli integral of motion,[32]

$$-\frac{\partial\phi}{\partial t}+\frac{1}{2}(\nabla\phi)^2+\frac{p(r,t)}{\rho}=-\frac{p_0(t)}{\rho}, \tag{9}$$

where $p_0(t)$ and $p(r,t)$ are the liquid's pressure at infinity and the pressure at any point in the liquid, respectively. The terms $\partial\phi/\partial t$ and $\nabla\phi$ can be calculated from Eq. (5), and with the boundary condition $r=R$, Eq. (9) finally gives the Rayleigh-Plesset equation,

$$R\ddot{R}+\frac{3}{2}\dot{R}^2=\frac{p(R,t)-p_0(t)}{\rho}. \tag{10}$$

Equation (10) is the general equation of motion for a spherical bubble in a liquid with a given pressure of surrounding liquid $p_0(t)$ and with the pressure on the bubble wall $p(R)$. In the special case when $p_0(t)-p(R,t)=$constant, it is easy to show that the identity

$$\frac{3}{2}\dot{R}^2+R\ddot{R}=\frac{1}{2\dot{R}R^2}\frac{d}{dt}(R^3\dot{R}^2), \tag{11}$$

gives the Rayleigh equation, Eq. (1). This means that the Rayleigh equation can also be used to describe a bubble's expansion.

The Rayleigh-Plesset equation, Eq. (10), can be further adapted by considering the viscosity of the liquid and the surface tension of the liquid in the pressure term $p(R)$.[32,35] Moreover, some authors expanded the theory of bubble dynamics by taking into account different effects, such as the compressibility of the liquid, the nonequilibrium condensation of the vapor, the heat conduction, and the temperature discontinuity at the phase interface.[36] However, for the interpretation of our experimental results it is important that Eq. (10), and also the derivative, can be rewritten in dimensionless form using the following normalization: $\xi=R/R_{\max}$ and $\tau=t/T_0$.[36]

III. EXPERIMENTAL SETUP

Two interconnected experimental setups were employed. This enabled a simultaneous application and, therefore, a comparison between the two techniques—BDP and shadow photography—for the measurements of bubble dynamics. The breakdown in distilled water was induced by a Q-switched Nd:YAG laser ($\lambda=1064$ nm) with a pulse duration of 7 ns designed for ocular photodisruption. The laser has an energy attenuator, which gave us the ability to operate at ten different energies. The bubble dynamics' measurements presented in this article were made at one of three laser energies: $8.6\times(1\pm0.3)$ mJ, $6.0\times(1\pm0.3)$ mJ, and $4.7\times(1\pm0.3)$ mJ, while the bubble's maximum radius was measured at two additional laser energies: $2.41\times(1\pm0.3)$ mJ and $1.63\times(1\pm0.3)$ mJ. Since the attenuator was placed in front of the laser optics, the beam characteristics did not depend on its position. The breakdown laser beam's waist radius in the water was ~30 μm, so the intensities in the experiments were in the range of $(1-4)\times10^{14}$ W m^{-2}. The measured threshold energy, E_{th}, for the laser-induced breakdown, i.e., the laser pulse's energy that corresponds to a 50% breakdown probability[37] in the distilled water used in this experiment, was $E_{\text{th}}=1.1\times(1\pm0.3)$ mJ.

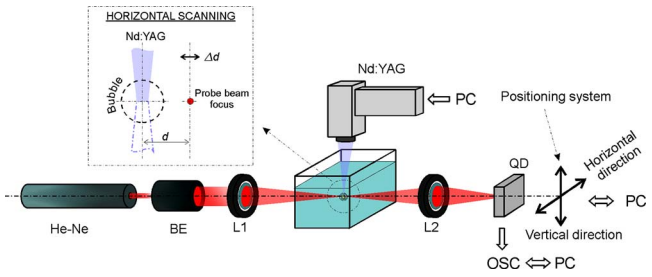

FIG. 1. Experimental setup for the BDP scanning. Breakdown was induced by the Nd:YAG pulsed laser. He-Ne laser was employed as a probe beam, led through lenses $L1$ and $L2$ into the fast quadrant photodiode QD. The positioning system enabled precise BDP scanning.

A. Beam-deflection probe measurements

The experimental setup for the BDP measurements is shown in Fig. 1. The breakdown, induced by the Nd:YAG laser, was detected with a photodiode used as an oscilloscope trigger. A He-Ne laser ($\lambda=633$ nm) was used as the probe beam. The beam was first focused ($L1$) into the vessel with the distilled water and then led through the lens $L2$ into the fast quadrant photodiode QD. The probe beam's waist radius was ~3 μm, while the rise time and the bandwidth of the quadrant photodiode were ~4 ns and ~200 MHz, respectively. The small beam diameter and the high-frequency bandwidth of the probe were necessary in order to achieve a high temporal as well as spatial resolution.

The laser-induced breakdown generates a shock wave and a cavitation bubble. The shock wave locally changes the density of the water and consequently its refractive index. On the other hand, in the case of a cavitation bubble the refractive-index gradient appears on its wall, representing the boundary between the steam and the surrounding water.[38] The refractive-index gradient results in the deflection of the probe beam,[39–41] which produces a signal from the photodetector. To ensure precise BDP measurements, the optical axes of the breakdown laser should lie in the probe beam's focal plane (see also the upper left-hand side of Fig. 1). Since we used a quadrant photodiode, accurate positioning of the probe beam relative to the point of the breakdown was possible. The quadrant photodiode records two signals corresponding to the horizontal and vertical probe-beam deflections. By considering both signals a relative position can be determined in the vertical as well as in the horizontal direction.

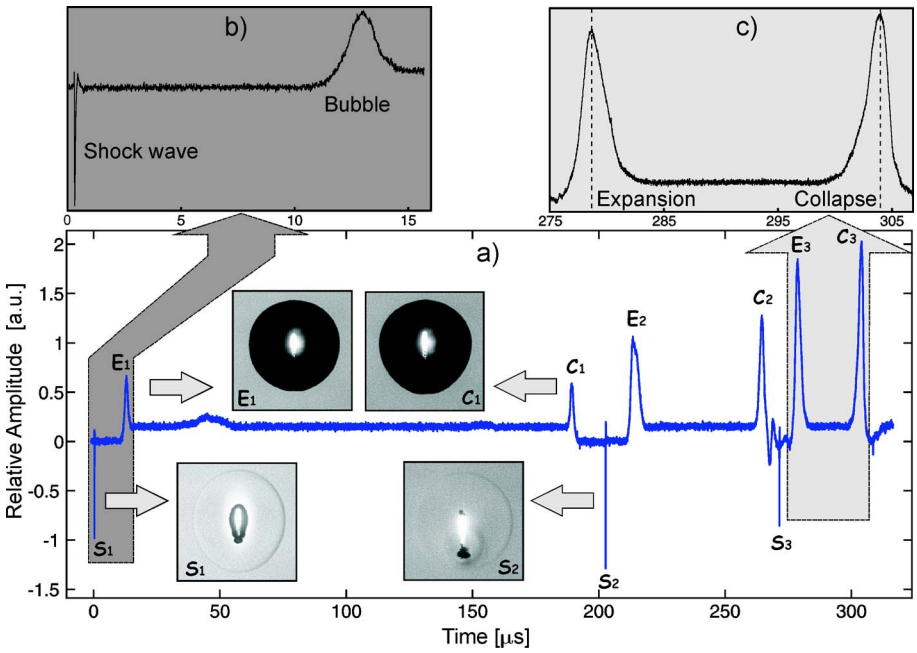

FIG. 2. (a) Typical BDP signal for a laser-pulse energy E_L=4.7 mJ. Peaks $E1$, $E2$, and $E3$ show the bubbles' expansions, while peaks $C1$, $C2$, and $C3$ correspond to their collapses. First shock wave immediately after breakdown results in the peak $S1$. Secondary shock waves were emitted after the bubble collapses and were detected as peaks $S2$ and $S3$. Shadow photography images are also shown: $S1$ and $S2$ correspond to the time when the shock waves were detected by the BDP (peaks $S1$ and $S2$). Images $E1$ and $C1$ show the cavitation bubble during the first expansion and the first collapse–BDP signal peaks $E1$ and $C1$. (b) Part of the signal as it appeared immediately after the breakdown. (c) Peaks due to the bubble's expansion and collapse.

The BDP measurements were made in the vertical as well as in the horizontal direction relative to the optical axes of the breakdown beam. The shift during scanning in both directions was 30 μm, while the shift used for measurements of the bubble's maximum radius was in the range of 10–30 μm. The applied positioning system for moving the laser probe beam relative to the breakdown region enabled a shift down to 1 μm. The experimental setup was automatically controlled with the specially developed software that also enabled data acquisition from a digital oscilloscope (500 MHz Wave Runner 6050A, LeCroy) as well as data processing.

B. Shadow photography measurements

Shadow photography[8,11,16,18] was used as a method for comparison during our experiments. A Nd:YAG pulsed laser (λ=1064 nm) with a pulse duration of 7 ns, which was led into a diffuser, was employed as the light source. The image was captured using a microscope equipped with a charge-coupled device (CCD) camera (1 M pixels, Basler A102f) and an interference filter (FWHM=10 nm). The microscope was adjusted in such a way that the spatial resolution was 4 μm per pixel.

Shadow photography, like BDP-based measurements, requires good repeatability of the process, while time-evolution measurements in a single shot require very sophisticated equipment (for the high-speed photography). The main difference between the BDP and shadow photography is as follows. With the BDP one can observe all of the bubble's dynamics at one point in space. This means that we can obtain information on all the expansions, collapses, and shock waves from the BDP signal. On the other hand, shadow photography enables two-dimensional measurements from a single shot. In principle its time resolution depends only on the pulse duration of the light source. Therefore, BDP scanning requires probe-beam position shifting relative to the breakdown region, while bubble dynamics measurements based on shadow photography require exposure-time delaying relative to the occurrence of the breakdown.

C. Typical signals

Figure 2(a) shows a typical BDP signal, recorded with the probe beam positioned at $d\sim500$ μm relative to the breakdown region. The breakdown laser energy was 4.7 mJ. Shortly after the breakdown ($t\sim0.5$ μs) the first peak, $S1$, appeared, showing the shock wave. The following peak, $E1$, was caused by a cavitation bubble during its expansion. The images from the shadow photography under equivalent conditions are also shown in the same figure (images $S1$ and $E1$). The bright area in the image $S1$ is plasma, the dark surrounding area is a cavitation bubble, while the "ring" surrounding the plasma and the bubble is a shock wave. In the image $E1$ the shock wave is not visible, since at that time ($\sim$13 μs) it was already out of the camera's field of view.

When the bubble reaches its maximum radius the surrounding liquid causes it to collapse. Therefore, the bubble's wall crosses the probe beam again at $t\sim190$ μs, resulting in the peak $C1$. During bubble collapse the pressure and temperature inside the bubble's wall increase up to values similar to those immediately after the breakdown.[36] This causes the expansion of a new bubble, and a secondary shock wave is emitted. Both phenomena can be seen in the BDP signal as the peaks $S2(t\sim200$ μs) and $E2(t\sim215$ μs). The corresponding images are also shown. The process repeats itself, resulting in bubble oscillations and detected as the peaks $C2$, $E2$, and $C3$, corresponding to the second collapse, the third expansion, and the third collapse of the bubble, respectively. The shock wave emitted after the second collapse was also detected as peak $S3$.

Figure 2(b) shows part of the signal as it appeared immediately after the breakdown. From the figure it is evident that the peak corresponding to the bubble is wider than the peak corresponding to the shock wave; the main reason for this is that the shock wave is much faster than the cavitation

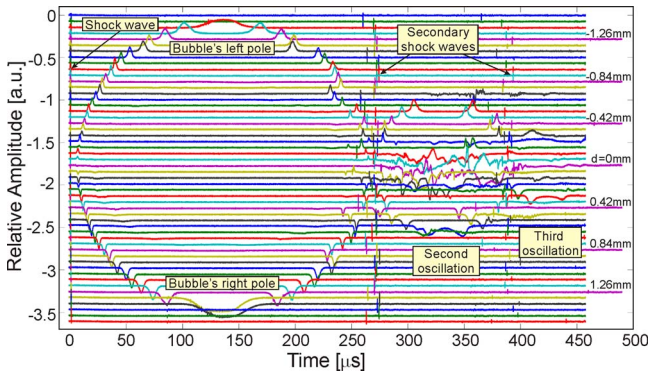

FIG. 3. Typical series of BDP signals during one-dimensional scanning. Sequence of signals corresponds to a total BDP shift of 3 mm; accordingly, each signal corresponds to a movement of the probe of 60 μm.

bubble. A detailed description of a BDP signal caused by a shock wave is reported elsewhere.[39–41] The peaks due to the bubble's expansion and collapse are shown in Fig. 2(c). It should be noted that these two signals are symmetrical about the vertical axis. When the bubble expands, the probe beam is first crossed by the outer boundary of the cavitation bubble, while during the collapse the inner side of the bubble intersects the BPD first. Therefore, the refractive-index profile is recorded in the opposite directions during the expansion and the collapse, respectively. This is in accordance with the described symmetry.

The cavitation bubble oscillations were monitored with one-dimensional BDP scanning. A typical series of signals from the BDP during horizontal scanning, i.e., perpendicular to the axis of the breakdown laser, is shown in Fig. 3. This was performed by changing the relative position of the probe beam and the breakdown region. The sequence of signals corresponds to a total BDP shift of 3 mm; accordingly, two consecutive signals from the graph correspond to a shift of 60 μm. Peaks corresponding to the first, second, and also third oscillations are clearly visible. The peaks appearing immediately after the breakdown represent the first shock wave; the peaks resulting from the secondary shock waves appear between 260 and 275 μs (second shock wave) and also between 380 and 400 μs (third shock wave). The maximum radius [Eq. (3)] and the bubble's collapse time [Eq. (2)] vary due to variations in the breakdown laser energy as well as the variation in the share of the laser energy converted into the mechanical energy of the bubble. Consequently, the peaks corresponding to the secondary shock wave are dispersed, since the secondary shock wave's emitting time coincides with the bubble's collapse. The left-hand peaks during each oscillation show bubble expansion, while the right-hand peaks show bubble collapse, and at the maximum radius of the bubble these two peaks merge into one. This phenomenon can be seen in the fourth signal from the bottom and the third signal from the top. During scanning the signal changes polarity when the probe beam crosses the breakdown region.

Shadow photography was used as a comparison during the experiments. A typical sequence of images is shown in Fig. 4; it corresponds to a laser energy of 8.6 mJ. The bright spot in the center shows light radiated from the plasma, which entered the camera despite the fact that a narrow bandpass filter was applied. The shock wave is also visible on the first six images ($A1-A6$). The cavitation bubble, visible as a black area on the bright background, expanded to its maximum radius at $t\sim 140$ μs (image $A9$) and then started to collapse. At time $t\sim 280$ μs (images $B4-B6$) one can see the secondary shock wave emitted as a result of the bubble's collapse. Later, the bubble expanded to its maximum radius for the second oscillation (image $B9$). The second collapse and the third shock wave followed at $t\sim 407$ μs (image $C3$). After the end of the oscillations the gas bubbles remained close to the breakdown region for a few seconds after the breakdown[37] and are visible in the last image ($C9$) of Fig. 4.

The cone shape of the bubble immediately after the breakdown, which is a consequence of the plasma shape and is described elsewhere,[8,37] was observed with the shadow photography, like the two-dimensional BDP scanning.

IV. RESULTS AND DISCUSSION

The oscillation time versus maximum radius for the first two oscillations obtained by our method is shown in Fig. 5 (points). The solid line represents Rayleigh's collapse time, as obtained from Eq. (2) for $p_0=1$ bar and $\rho=10^3$ kg m^{-3}. It is clear that this relatively simple model is in good agreement with our measurements as well as with the results obtained by others.[26] The measured maximum radii of the bubbles were in the range 0.8 ± 0.05 mm (for laser energy

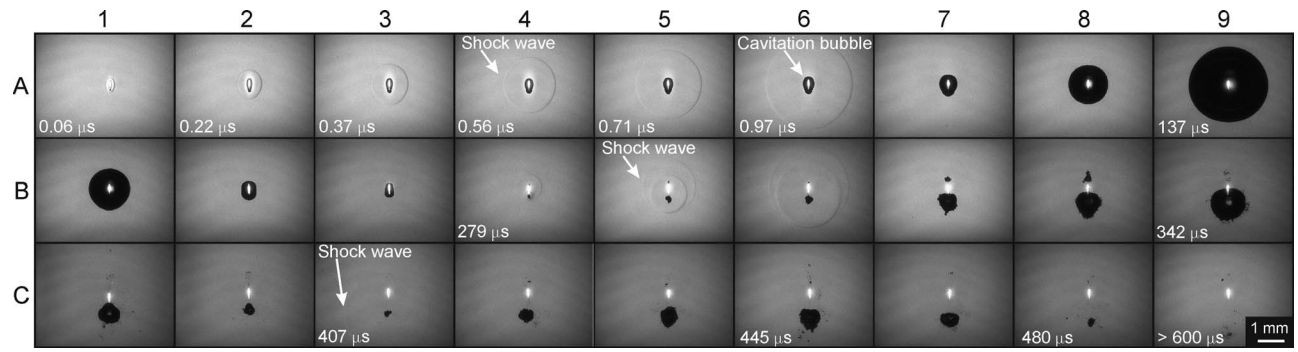

FIG. 4. Typical sequence of cavitation-bubble images made by shadow photography. The laser pulse with an energy $E_L=8.6$ mJ and a duration of 7 ns is entering from the top of each image. Bright spot in the center shows light radiated from the plasma, while the black area on the bright background shows the cavitation bubble. Sshock wave is visible as a "ring" surrounding the plasma and the bubble. Time relative to the occurrence of breakdown is shown on the images.

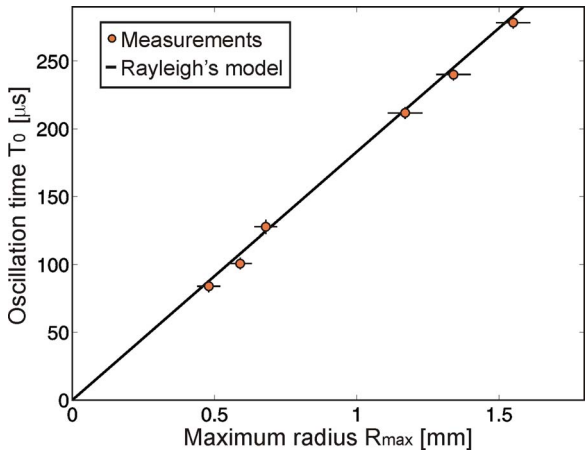

FIG. 5. Oscillation time vs maximum radius for first two bubble's oscillations (points) and three different laser-pulse energies. Rayleigh's model [see Eq. (2)] for $p_0=1$ bar and $\rho=10^3$ kg m^{-3} is also shown (solid line).

$E_L=1.63\pm0.04$ mJ) and 1.55 ± 0.06 mm (for laser energy $E_L=8.6\pm0.23$ mJ) and are in accordance with the results obtained by other authors[12] who used high-speed photography.

Equations (3) and (4) were verified by maximum-radii measurements at different laser-pulse energies. The results were in good agreement with theory, as previously reported by other authors.[7] On this basis we were able to calculate the share of the laser-pulse energy converted into the mechanical energy of the cavitation bubble E_{b1}. The results are presented in Table I; they show that the share η of the optical energy converted into the bubble energy is in the range 14–18%.

From the radii measurements we also calculated the energies of the second and the third bubbles' oscillations. The results are presented in Table I, where the shares of the first oscillation energy converted into the energy of the second E_{b2}/E_{b1}, and the third oscillation E_{b3}/E_{b1} are also shown. The bubble energy is lost due to the emission of a shock wave after every collapse, the heat conduction, and the liquid's viscosity. Vogel *et al.*[17] found that the energy loss due to the emission of a shock wave represents between 70% and 90% of the energy losses. Therefore, from the results presented in Table I, the energies carried off with the second and third shock waves can be estimated as 64–84% and 4–6% of the first bubble's oscillation, respectively. From the application point of view, shock-wave energy is important since its range—in contrast to that of the cavitation bubble—is not limited to the vicinity of the breakdown region.

A. Method for reducing the measurement noise of the BDP scanning technique

During the scanning procedure the energy of the cavitation bubble varies from pulse to pulse. This variation appears because of the laser pulse's energy variation as well as the variation in the share of the pulse energy converted into the bubble energy. As has already been shown, the bubble's radius [see Eq. (3)] and consequently the oscillation time [see Eq. (2)] strongly depends on its energy. In the case of measurements using the BDP, it means that the time needed for the bubble to reach the current position of the probe beam varies. These bubble-energy variations lead to the measurement noise that is visible in Fig. 7(a). In this section we propose a method for reducing this measurement noise. The method is based on a unique property of the BDP: that during measurements at each particular position it simultaneously gives information about oscillations times. The oscillations times can be obtained from a single BDP signal by analyzing the peaks that correspond to the shock waves that are emitted after breakdown and after each collapse. The method also relies on the Rayleigh-Plesset model of cavitation bubbles, as described in Sec. II. A detailed description of the method follows.

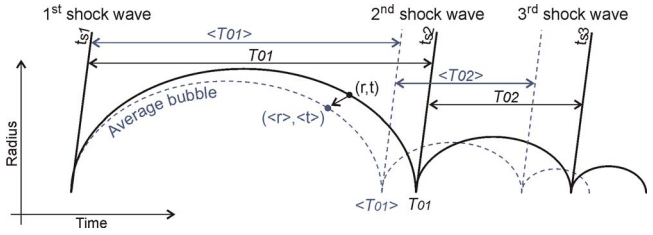

FIG. 6. Schematic diagram of the principle of the method for reducing the measurement noise of the BDP scanning. Method is based on considering the secondary shock waves. It gives the transformation of the measured bubble's coordinates (t,r) into the corresponding coordinates of an average bubble $(\langle t\rangle,\langle r\rangle)$. Here, the oscillation times for the first and the second bubble's oscillations are denoted as $\langle T_{01}\rangle$ and $\langle T_{02}\rangle$ for an average bubble and as T_{01} and T_{02} for a measured bubble.

The difference in the time of flight for the second shock wave t_{S2} and the time of flight for the first shock wave t_{S1} equals the first oscillation time T_{01}, as is schematically shown in Fig. 6. Similarly, the difference between the time of flight for the third shock wave t_{S3} and the time of flight for the second shock wave t_{S2} emitted from the same bubble equals the oscillation time of the second oscillation T_{02}. Therefore, an average oscillation time for the first as well as for the second oscillation can be deduced as an arithmetic mean of the time-of-flight differences,

$$\langle T_{01}\rangle = \frac{1}{N}\sum_{i=1}^{N}(t_{S2i}-t_{S1i}), \tag{12}$$

TABLE I. Calculated energies for the first (E_{b1}), second (E_{b2}), and third (E_{b3}) oscillations. The shares of the laser-pulse energy converted into the bubble energy η, as well as the shares of the first bubble's energy converted into the energy of the second and the third oscillations, are also shown.

E_L[mJ]	$E_{b1}[\mu J]$	η	$E_{b2}[\mu J]$	E_{b2}/E_{b1}	$E_{b3}[\mu J]$	E_{b3}/E_{b1}
8.60±0.23	1500±180	18%±3%	129±23	8.4%±3%	24±6	1.6%±0.7%
6.0±0.12	980±130	16%±3%	84±17	8.5%±3%	13±4	1.4%±0.7%
4.7±0.16	660±100	14%±3%	45±11	6.9%±3%	6±2	1.0%±0.6%

$$\langle T_{02}\rangle = \frac{1}{N}\sum_{i=1}^{N}(t_{S3i} - t_{S2i}), \tag{13}$$

where i denotes successive measurements.

In dimensionless form (parameters $\xi = r/R_{\max}$ and $\tau = t/T_0$), all the bubbles have the same shape. Therefore, the ratio between the current measured time and the measured oscillation time is equal to the ratio of the average current time to the average oscillation time,

$$\frac{t}{T_0} = \frac{\langle t\rangle}{\langle T_0\rangle}. \tag{14}$$

An analogous relation can be applied to the current radius and the average radius,

$$\frac{r}{R_{\max}} = \frac{\langle r\rangle}{\langle R_{\max}\rangle}. \tag{15}$$

Here, r and t are the measured bubble's current coordinate, while $\langle r\rangle$ and $\langle t\rangle$ correspond to the coordinate of an average bubble. Since $R_{\max}$ is proportional to T_0, the transformation from the coordinate of the measured bubble (t,r) into the average bubble coordinates $(\langle t\rangle,\langle r\rangle)$ in the case of the first oscillation can be written as

$$(\langle t\rangle,\langle r\rangle) = \frac{\langle T_{01}\rangle}{T_{01}}(t,r). \tag{16}$$

In the case of the second oscillation the method can be applied in a similar way by considering the third shock wave. The only difference in this case is that the oscillation time for the first oscillation should be subtracted from the measured time of flight first, and then the average oscillation time for the first oscillation should be added, so

$$\langle t\rangle = \frac{\langle T_{02}\rangle}{T_{02}}(t - T_{01}) + \langle T_{01}\rangle, \tag{17}$$

$$\langle r\rangle = \frac{\langle T_{02}\rangle}{T_{02}}r. \tag{18}$$

Applying it to the third oscillation would require a fourth shock wave; however, this wave did not appear during our experiments, or it appeared in only a few cases. Therefore, in this case the measurement noise can be reduced by correcting the measured times of flight for the third oscillation as follows. The third shock wave corresponding to the start of the third oscillation can be aligned relative to the first shock wave, so

$$\langle t\rangle = t - [t_{S3} - (\langle T_{01}\rangle + \langle T_{02}\rangle)], \tag{19}$$

$$\langle r\rangle = r. \tag{20}$$

We also found that the majority of the measurement noise arises from the variation in the share of the energy converted from optical energy into the mechanical energy of the bubble, as well as the share of the energy converted between the bubble's oscillation energies. During the experiments we simultaneously measured the laser-pulse energy. Therefore, the measurement noise due to the variation in the laser-pulse energy should be reduced by considering Eq. (3), as follows.

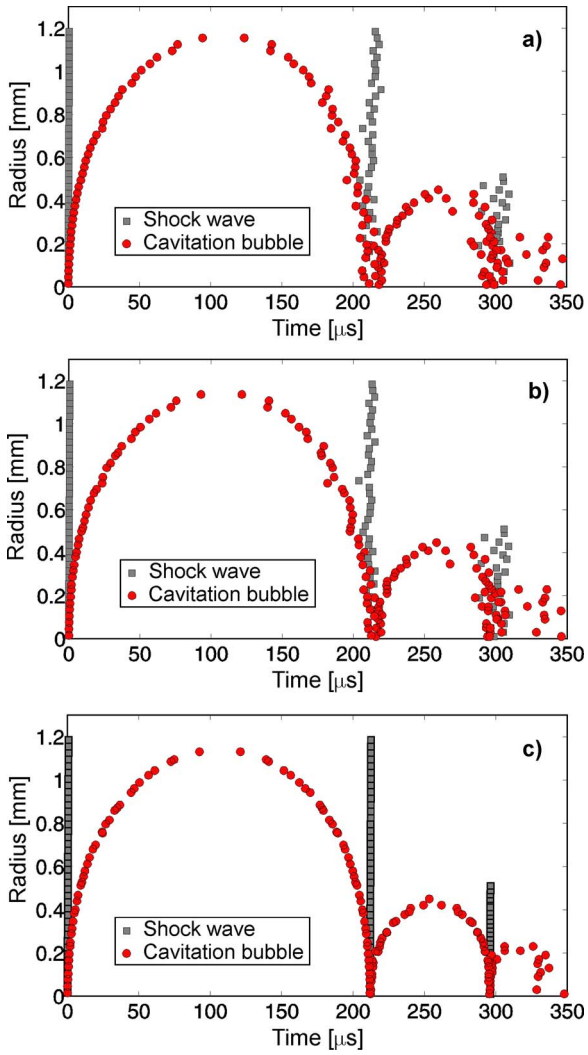

FIG. 7. (a) Results of cavitation-bubble measurements using BDP scanning. Energy of the breakdown laser was 4.7 mJ. (b) Same results after considering the variations in the breakdown laser's energy. (c) Same results obtained using the method for reducing the measurement noise of the BDP scanning based on analyzing the secondary shock waves.

The transformation from the coordinate of the measured bubble (t,r) into the average bubble's coordinates $(\langle t\rangle,\langle r\rangle)$ can be deduced from Eqs. (14) and (15) and a Taylor series expansion of Eq. (3); therefore

$$(\langle t\rangle,\langle r\rangle) = \left(1 - \frac{1}{3}\frac{\Delta E}{\langle E\rangle}\right)(t,r). \tag{21}$$

Here, ΔE is the difference between the measured energy E and the mean energy $\langle E\rangle$.

Figure 7 shows results (for $E_L = 4.7$ mJ) obtained using the BDP technique [Fig. 7(a)] as well as the results obtained by considering the variation in the breakdown laser energy [Fig. 7(b)] and the results from the method for reducing the measurement noise [Fig. 7(c)], respectively. In Fig. 7(b), which shows the results obtained by using Eq. (21), it is clear that the measurement-noise reduction for this case is barely visible. On the other hand, the measurement noise is significantly reduced by the method that considers the secondary shock waves [see Fig. 7(c)]. Therefore, it can be concluded

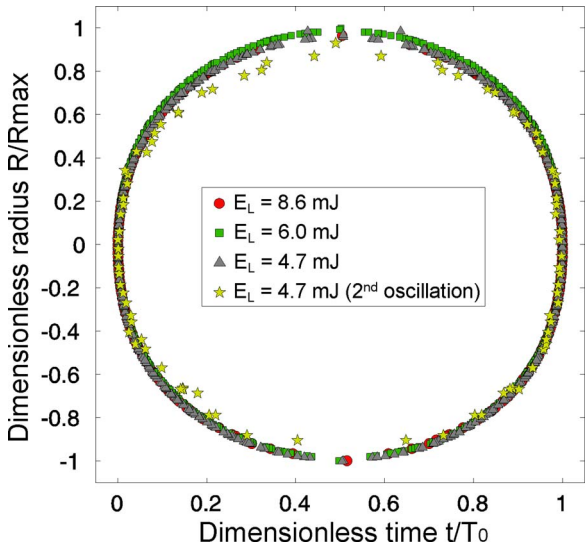

FIG. 8. Dimensionless radii vs dimensionless time are shown for the first oscillation (at laser energies E_L=8.6, 6.0, and 4.7 mJ) as well as the second oscillation at E_L=4.7 mJ. Experimental data show good agreement with the theoretical predictions of the Rayleigh-Plesset model. This justifies the application of the method for reducing the measurement noise due to BDP scanning.

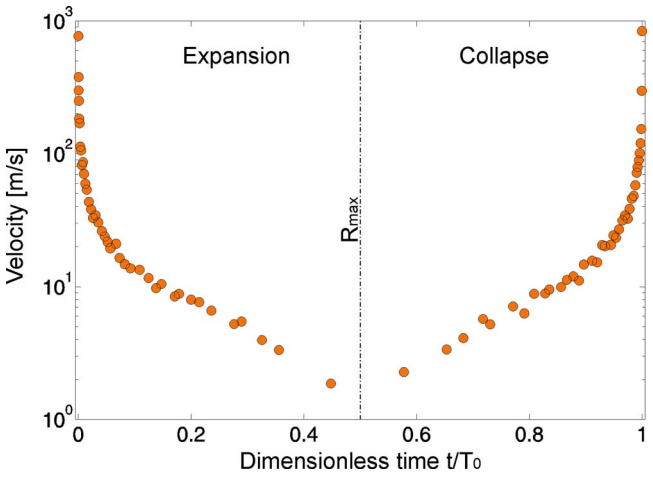

FIG. 9. Velocity as a function of dimensionless time is shown for the bubble's expansion and collapse. A logarithmic scale is used on the vertical axis.

that the variation in the breakdown laser energy did not represent a major contribution to the measurement noise.

An experimental confirmation of the theoretical predictions of the equivalent bubble's shape on a dimensionless graph is shown in Fig. 8. It shows the results for the first oscillations recorded at three laser-pulse energies, E_L=8.6, 6.0, and 4.7 mJ, and also the second oscillation recorded at the laser-pulse energy E_L=4.7 mJ.

Typical results for the presented method can be seen in Fig. 9. It shows the velocities for a laser-induced cavitation bubble in distilled water and their dependence on dimensionless time. It is important to notice that a logarithmic scale is used on the vertical axis. If the bubbles have the same shape, their velocities should be the same, since velocity represents the slope of the radius curve. It is easy to see that the velocity decreases rapidly. The measured velocity at $(14\pm4)\times10^{-5}$ T_0 after the breakdown is ~780 m s^{-1}, while at $(39\pm8)\times10^{-5}$ T_0 the velocity is only ~300 m s^{-1}. After 0.14 T_0 the velocity is below 10 m s^{-1}. The results are in accordance with those reported by other authors[8] who used shadow photography.

B. Comparison between BDP and shadow photography

Figure 10 shows the comparison between results obtained from the BDP using the method for reducing measurement noise based on the scanning procedure (circles) and the results obtained from the shadow photography (deltoids). The comparison is shown for the laser-pulse energy E_L =8.6 mJ. In the case of the shadow photography the bubbles' radii were obtained from analyzing images. Figure 10(a) shows the radius versus time measured with both methods. The velocities, calculated from radius measurements,

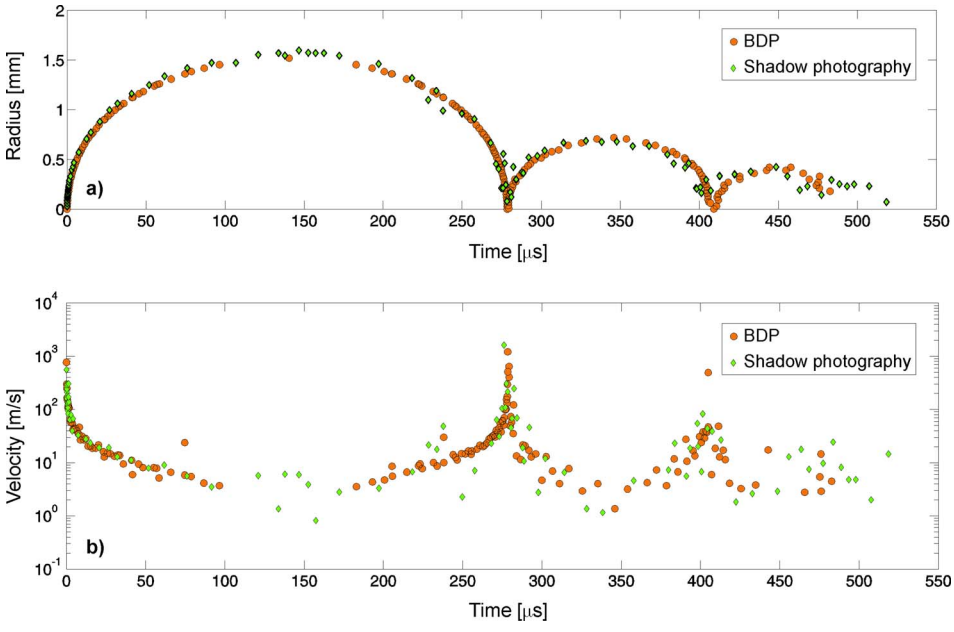

FIG. 10. Comparison between the results obtained from the BDP using the method for reducing the measurement noise (circles) and the results obtained from the shadow photography (deltoids). Laser-pulse energy was 8.6 mJ.

are shown in Fig. 10(b). It is clear that there is good agreement between the methods, and that there is less measurement noise associated with the BDP measurements.

V. CONCLUSION

We have presented measurements on laser-induced cavitation bubbles using a laser-beam deflection probe (BDP) and shadow photography. The latter method was used for a comparison during our experiments and demonstrated the good agreement of both methods. The scanning technique based on the BDP and the time-evolution measurements based on the shadow photography produced measurement noise due to the repetition of the process. For this reason we developed a method based on an analysis of the secondary shock waves in order to reduce this measurement noise. This improved technique uses a unique property of BDP: all the cavitation bubble's oscillations and shock waves can be obtained from a single BDP signal. We showed that such a method significantly reduces the measurement noise, and as a result it can be used as an alternative to high-speed photography, which requires very sophisticated equipment.

A comparison was made between the results obtained by using the BDP technique, the results obtained from considering the variation of the breakdown laser energy, and the results obtained with the method for reducing the measurement noise. We showed that the majority of the measurement noise arises from the variation in the share of the energy conversion from optical energy into the mechanical energy of the bubble, as well as from the first oscillation's energy into the energy of the subsequent oscillations.

ACKNOWLEDGMENT

We would like to thank Optotek d.o.o. for supplying the *Q*-switched Nd:YAG photodisruptor laser (OptoYAG) used as a breakdown laser in our experiments.

[1] W. Lauterborn and H. Bolle, J. Fluid Mech. **72**, 391 (1975).
[2] A. Philipp and W. Lauterborn, J. Fluid Mech. **361**, 75 (1998).
[3] E. A. Brujan, K. Nahen, P. Schmidt, and A. Vogel, J. Fluid Mech. **433**, 251 (2001).
[4] W. D. Song, M. H. Hong, B. Lukyanchuk, and T. C. Chong, J. Appl. Phys. **95**, 2952 (2004).
[5] S. V. Egerev, Acoust. Phys. **49**, 59 (2003).
[6] J. R. Krieger and G. L. Chahine, J. Acoust. Soc. Am. **118**, 2961 (2005).
[7] A. Vogel, P. Schweiger, A. Frieser, M. N. Asiyo, and R. Bringruber, IEEE J. Quantum Electron. **26**, 2240 (1990).
[8] A. Vogel, S. Busch, and U. Parlitz, J. Acoust. Soc. Am. **100**, 148 (1996).
[9] E. A. Brujan, K. Nahen, P. Schmidt, and A. Vogel, J. Fluid Mech. **433**, 283 (2001).
[10] R. Petkovšek, J. Možina, and G. Močnik, Opt. Express **13**, 4107 (2005).
[11] I. Apitz and A. Vogel, Appl. Phys. A: Mater. Sci. Process. **81**, 329 (2005).
[12] E. A. Brujan and A. Vogel, J. Fluid Mech. **558**, 281 (2006).
[13] P. Marmottant and S. Hilgenfeldt, Nature **423**, 153 (2003).
[14] P. Prentice, A. Cuschieri, K. Dholakia, M. Prausnitz, and P. Campbell, Nat. Phys. **1**, 107 (2005).
[15] W. Lauterborn, Appl. Phys. Lett. **21**, 27 (1972).
[16] D. C. Emmony, T. Geerken, and H. Klein-Baltink, J. Acoust. Soc. Am. **73**, 220 (1983).
[17] A. Vogel, W. Lauterborn, and R. Timm, J. Fluid Mech. **206**, 299 (1989).
[18] J. Noack, D. X. Hammer, G. D. Noojin, B. A. Rockwell, and A. Vogel, J. Appl. Phys. **83**, 7488 (1998).
[19] J. Noack and A. Vogel, Appl. Opt. **37**, 4092 (1998).
[20] Y. Tomita and T. Kodama, J. Appl. Phys. **94**, 2809 (2003).
[21] G. N. Sankin, W. N. Simmons, S. L. Zhu, and P. Zhong, Phys. Rev. Lett. **95**, 034501 (2005).
[22] R. Petkovšek, G. Močnik, and J. Možina, Fluid Phase Equilib. **256**, 158 (2007).
[23] T. Kurz, D. Kröninger, R. Geisler, and W. Lauterborn, Phys. Rev. E **74**, 066307 (2006).
[24] W. Lauterborn and A. Koch, Phys. Rev. A **35**, 1974 (1987).
[25] E. Herbert, S. Balibar, and F. Caupin, Phys. Rev. E **74**, 041603 (2006).
[26] D. Obreschkow, P. Kobel, N. Dorsaz, A. de Bosset, C. Nicollier, and M. Farhat, Phys. Rev. Lett. **97**, 094502 (2006).
[27] Y. Tomita and A. Shima, J. Fluid Mech. **169**, 535 (1986).
[28] A. Vogel, I. Apitz, S. Freidank, and R. Dijkink, Opt. Lett. **31**, 1812 (2006).
[29] Z. W. Liu, G. J. Steckman, and D. Psaltis, Appl. Phys. Lett. **80**, 731 (2002).
[30] H. K. Park, D. Kim, C. P. Grigoropoulos, and A. C. Tam, J. Appl. Phys. **80**, 4072 (1996).
[31] L. Rayleigh, Philos. Mag. **34**, 94 (1917).
[32] M. S. Plesset, J. Appl. Mech. **16**, 277 (1949).
[33] A. Vogel, J. Noack, K. Nahen, D. Theisen, S. Busch, U. Parlitz, D. X. Hammer, G. D. Noojin, B. A. Rockwell, and R. Birngruber, Appl. Phys. B **68**, 271 (1999).
[34] Y. Tomita, M. Tsubota, and N. An-Naka, J. Appl. Phys. **93**, 3039 (2003).
[35] A. Shima, Shock Waves **7**, 33 (1997).
[36] S. Fujikawa and T. Akamatsu, J. Fluid Mech. **97**, 481 (1980).
[37] A. Vogel, K. Nahen, D. Theisen, and J. Noack, IEEE J. Sel. Top. Quantum Electron. **2**, 847 (1996).
[38] A. Vogel, *Optical Breakdown in Water and Ocular Media, and Its Use for Intraocular Photodisruption* (Shaker, Aachen, Germany, 2001).
[39] G. P. Davidson and D. C. Emmony, J. Phys. E: J. Sci. Instrum. **13**, 92 (1980).
[40] J. Diaci, Rev. Sci. Instrum. **63**, 5306 (1992).
[41] J. Diaci and J. Možina, Rev. Sci. Instrum. **66**, 4644 (1995).